

The Breakdown Mechanism of Diamond Like Carbon Coated Nickel in Chloride Solution

R.S. Lillard, D.P. Butt, T.N. Taylor, K.C. Walter, M. Nastasi

Materials Science and Technology Division

The Los Alamos National Laboratory

Los Alamos, New Mexico 87545

Abstract

The breakdown mechanism of chemical vapor deposited nickel (CVD Ni) coated with 5 micrometers of diamond like carbon (DLC) produced by plasma source ion implantation (PSII) in chloride solution was investigated. PSII differs from traditional implantation techniques in that the targets are placed directly in a plasma source and then pulse biased to produce a non-line-of-sight process to complex-shaped targets without complex fixturing. Electrochemical Impedance Spectroscopy (EIS) measurements indicated the presence of small pores in the DLC presumably formed in the deposition process. These pores were also observed in the scanning electron microscope. These pores exposed a layer of CVD Ni implanted with carbon (C) prior to depositing the DLC. Therefore, EIS results were analyzed within the context of an equivalent circuit model which incorporated three time constants representing the Ni-C implant layer, the DLC/solution interface, and the pore/solution interface. Good correlation between CNLS fitting of the impedance data and this circuit model was obtained. Upon immersion in chloride solution, the onset of breakdown of the DLC coating was rapid. However, breakdown failed to initiate in chloride solution buffered with sodium borate. Mixed potential theory was used to describe these results and mechanisms for the initiation and propagation of coating failure in chloride solutions.

key words: corrosion, diamond like carbon, coatings, chemical vapor deposited nickel, chloride, electrochemical impedance spectroscopy, ion implantation, surface modification

Introduction

There currently exists a broad range of applications for which the ability to produce an adherent, hard, wear and, corrosion-resistant coating plays a vital role. These applications include engine components, orthopedic devices, textile manufacturing components, hard disk media, optical coatings, and cutting and machining tools (e.g., punches, taps, scoring dies, and extrusion dies). Plasma-based ion beam processing can play an important role in all of these technologies. The ability to provide flux, energy, and temporal control of a variety of ions, provides an avenue to tailor surface structure and chemistry necessary to solve current and future problems related to corrosion, surface hardness and tribological properties. Ion implantation is a well established ion beam based surface modification technique which has been successfully used to enhance materials engineering performance in areas such as, hardness[1], friction and wear[2], fracture toughness, and corrosion [3,4,5,6].

Corrosion studies involving ion implantation fall into two principle categories: (a) studies of novel surface alloys and (b) attempts to improve the corrosion resistance of some commonly used engineering alloys. Table 1 lists some examples of corrosion studies performed on ion implanted surface alloys[7,8,9,10,11,12]. The enhanced resistance to corrosion which many ion implanted materials exhibit is generally attributed to the ability to produce a surface layer which is both supersaturated with respect to the solubility limit of the alloy addition and free from second phase particles. Chemical homogeneity in single phase alloys is also a benefit. Second phase precipitates are undesirable as they are often more noble than the matrix and, therefore, tend to promote localized corrosion. Ion implantation also offers some scope for the formation of amorphous surface alloys. Amorphous alloys formed by rapid quenching often exhibit superior corrosion resistance provided that the alloy has a sufficient concentration of a strong passivator such as Cr. In spite of the flexibility and promise of this technique, ion implantation has been considered too expensive or impractical for mass production applications

Plasma source ion implantation (PSII), has the potential to overcome the limitations of conventional ion implantation by: (1) reducing the time and expense for implanting complex shapes and large areas and (2) extending the thickness of the modification zone through ion beam

enhanced plasma growth of surface coatings. In PSII, targets are placed directly in a plasma source and then pulse biased to produce a non-line-of-sight process for complex-shaped targets without complex fixturing. If the pulse bias is a relatively high negative potential (20 to 100 kV) ion implantation will result. If however, a low voltage (50 - 1200 eV) high duty cycle pulse bias is applied, film deposition from the chamber gas will result, thereby increasing the extent of the surface modification into the 1–10 micron regime.

Diamond like carbon (DLC) coatings have been successfully deposited by other investigators with traditional ion beam techniques[13,14]. In this study, DLC coating was deposited by PSII onto chemical vapor nickel (CVD Ni). CVD Ni was chosen for a substrate as it was a candidate for neutron detector housings which are to be constructed for the Sudbury Neutrino Observatory[15]. These detectors will be exposed to chloride solution during normal operating conditions. To evaluate the potential for DLC to be used as a corrosion barrier, Electrochemical Impedance Spectroscopy (EIS) and traditional electrochemistry techniques were used to investigate the break down mechanism in chloride and nonchloride containing environments. The effect of surface preparation on coating breakdown was also evaluated.

Experimental

High purity CVD Ni was made from the thermal decomposition of nickel carbonyl ($\text{Ni}(\text{CO})_4$). The resultant CVD Ni sheet was laser machined into 1.59 cm diameter disks approximately 0.065 cm thick. These samples were polished to a 0.30 μm finish. The polished CVD Ni samples were placed in an ion implantation chamber where the native oxide was removed by sputter etching with argon (Ar) for one hour. This sputter cleaning was immediately followed by carbon (C) implantation from methane at 30 kV. Carbon implantation prior to coating with DLC improves the adhesion properties of the DLC. After implantation, the surface was sputter cleaned for approximately 15 minutes. DLC was then deposited onto this surface from an RF plasma of acetylene (4.5 mTorr total pressure). The final DLC thickness was approximately 4-5 microns[16]. Transmission electron microscopy of similar specimens have shown the DLC structure to be amorphous[17]. The DLC coating had a density of 1.9 g/cm^3 and consisted of

approximately 70 at% C and 30 at% hydrogen (H). The C:H ratio was found to greatly effect coating properties with lower hydrogen content yielding coatings with the highest hardness values. The C:H ratio also effected coating resistivity and adhesion. The hardness of the DLC coatings examined was found to be to directly proportional to sp³ content. The sp³ contents of these coatings varied between 55% and (20%) and the hardness values between 6 and 12 GPa[18].

Corrosion experiments were conducted in 3 solutions: 1) 0.5M boric acid / 0.05M sodium borate pH 7.2, 2) 0.25M NaCl pH 7.0 and, 3) 1.0M NiCl₂ (2N Cl⁻) pH 6.1. Some solutions were deaerated with ultra-high purity Ar for at least 18 hours prior to the immersion of the test sample into the solution. For solutions containing chloride (Cl⁻) a Saturated Calomel Electrode (SCE; +0.241 vs. Normal Hydrogen Electrode) was used as a reference. For non Cl⁻ containing solutions, a Mercury / Mercury - Sulfate Electrode (MMSE; +0.375V vs. SCE) was used as a reference to prevent contamination of the solution with Cl⁻. Where necessary, potentials measured with MMSE are shown in this paper on the SCE scale for continuity.

EIS experiments were conducted at the Open Circuit Potential (OCP) over the frequency range of 1x10⁻² - 4.0x10⁴ Hz. Data were collected in this frequency range at 10 points per decade of frequency. Prior to EIS measurements the OCP was monitored for 1 hour to insure steady state. Anodic and cathodic polarization curves were generated at a sweep rate of 0.1 mV/sec after 1 hour at the OCP to insure steady state.

Surface composition and bonding states were measured using Auger electron spectroscopy (AES) and x-ray photoelectron spectroscopy (XPS) in conjunction with argon ion sputter profiling. Both of these spectroscopic methods were afforded by a Physical Electronics 5600ci multi-technique analytical apparatus. The XPS was done using a monochromatized AlK_α x-ray source, the high resolution spectra being acquired at 58.7 eV pass energy with an analyzer aperture setting of 800 microns. The spectrometer energy scale was calibrated to give Au 4f_{7/2} and Cu 2p_{3/2} peak positions within 0.05 eV of 84.0 and 932.65 eV binding energy, respectively[19]. Auger measurements were made using 3000 eV incident energy electrons. Sputtering profiling was done in an XPS mode by rastering 4000 eV Ar ions over a (4 x 4) mm² area. No electron

beam degradation was detected during the course of the Auger measurements. However, the sputtering process is undoubtedly responsible for some alteration or degradation of the bonding configuration.

Results and Discussion

Characterization of DLC in Chloride Solution and EIS Model Chemical vapor deposited Ni samples coated with DLC were exposed to deaerated 0.25M NaCl solution (pH 7). The EIS data as a function of immersion time are presented in Figures 1a and 1b in the form of Bode magnitude and phase plots for a 28 hour period. As seen in Figure 1b, the phase data fall below -45° at three separate frequencies. These frequencies shall be referred to as break points. They are most easily observed in the 24 hr data: f_H at approximately 9×10^3 Hz, f_L at approximately 0.03 Hz, and an intermediate break point (f_I) at approximately 158 Hz. As the time of immersion increases, both f_H and f_I progressively increase. Upon removal from solution, large corrosion pits in the DLC could be easily seen. These pits were approximately 0.40 mm in diameter and had propagated between 60 and 100 μm into the CVD Ni (Figure 2a and 2b). As shown in Figure 2a, the pit edges (formed by the DLC) were sharp and, in some instances, contained angular points of intersection. This suggests that the DLC surface did not react electrochemically, but instead broke away as a result of increased surface tension associated with undermining of the film due to Ni corrosion. This undermining effect can also be seen in Figure 2b.

The EIS response of the DLC / CVD-Ni samples in chloride solution is best modeled by an equivalent circuit (EC) first proposed by Hitzig[20] and later observed by Mansfeld[21] for anodized aluminum (Figure 3). In our system the intrinsic electrical properties of the carbon implanted layer are represented by the elements C_{IL}^i and R_{IL}^i , where the superscript ‘i’ represents “intrinsic”. This layer acts in series with the DLC coating represented by the elements C_{DLC}^i and R_{DLC}^i which model the capacitance and charge transfer resistance of the DLC. The elements representing the carbon implanted layer and DLC act in parallel with small “pinholes” in the DLC (less than $20\mu\text{m}$ in diameter; Figure 3a). These pinholes expose either the carbon implanted layer, a very thin DLC layer or, a combination of both. As will be shown later in this paper, these pinholes act as initiation sites for breakdown and are, therefore, associated with a double layer

capacitance and corrosion resistance, C_{dl}^i and R_{corr}^i respectively. The fraction of surface covered by these pinholes is defined by Θ and the fraction of surface covered by DLC is defined by $1-\Theta$. The observed (measured with EIS) parameters will necessarily scale with Θ . These ‘observed’ elements are represented by a superscript ‘o’. For example: $R_{corr}^o = R_{corr}^i/\Theta$ and $R_{DLC}^o = R_{DLC}^i/(1-\Theta)$.

Complex non-linear least squares fitting (CNLS) of the experimental DLC data taken after 24 hours of immersion in 0.25M NaCl to the EC presented in Figure 3a is presented in Figure 4a and 4b. As shown in these figures good correlation between the fit and measured data was always observed (for clarity, not all of the experimental data points are shown). The parameters R_{corr}^o and C_{dl}^o from the CNLS fit for DLC data are presented in Table 2. By measuring the final defect area, Θ^f (approximately $1 \times 10^{-3} \text{ cm}^2$), in a scanning electron microscope, the fraction of the surface area covered by defects as a function of immersion time was determined from the relationship:

$$\frac{\Theta^t}{\Theta^f} = \frac{R_{corr}^f}{R_{corr}^t} \quad \text{Eq.1}$$

where: Θ^t is the fraction of the surface area covered by defects at time t, R_{corr}^t is the resistance of the defect (R_{corr}^o) at time t, and R_{corr}^f is the final observed defect resistance. In accordance with Mansfeld[21], the change in f_i and f_L as a function of immersion time can be correlated with the fraction of the DLC surface covered by defects, Θ (where $1-\Theta$ is equal to the fraction of the surface covered by DLC, Figure 3b). As shown in Table 2, little or no change in R_{IL}^o is observed during the test period. Because R_{IL}^o is inversely proportional to $1-\Theta$ (Figure 3a), for small changes in Θ R_{IL}^o remains relatively unchanged. Similarly, the charge transfer resistance associated with the DLC is inversely proportional to $1-\Theta$ and, for small changes in R_{DLC}^o remains fairly constant as a function of immersion time. The large changes in R_{corr}^o observed during the 24 hr. immersion test period are attributed to *relatively* large changes in Θ . This correlates well with the large corrosion pits observed in the DLC CVD Ni sample after removing it from the NaCl solution. A decrease in the intrinsic value of R_{corr}^i with immersion time may alternatively explain the observed decrease in R_{corr}^o . By this same reasoning, Θ may be in error if R_{corr}^i decreased as a function of immersion

time. However, this explanation is unlikely for R_{corr}^{-1} because of the large corrosion rates (small resistances) measured and in contrast to the observed corrosion pits.

Initial Coating Properties Upon immersion in 0.5M boric acid / 0.05M sodium borate solution the OCP of the DLC CVD Ni sample decreased from approximately 0.0V SCE to a steady state value of -0.225V SCE within approximately 1 hour. During the test period for this sample (4 days), the OCP never deviated more than 0.03V from this potential. The Bode magnitude and phase data for this sample taken at the OCP after 1 hour of immersion and after 4 days of immersion are presented in Figures 5a and 5b respectively. As seen in these figures the day 4 data differs little from that on day 1. No change in f_{H} at approximately 10^4 Hz or f_{L} at approximately 10^{-1} Hz is observed during this time period. Further, no clear distinction between f_{H} , and f_{I} is apparent.

After 4 days of immersion in deaerated boric acid / sodium borate buffer solution, enough sodium chloride was added to the existing solution such that the Cl^- concentration reached 0.25M. After the OCP of the DLC coated CVD Ni sample reached steady state, (-0.217V SCE, approximately 1 hr), EIS data were taken. The Bode magnitude and phase plots are presented in Figure 6a and 6b. Also presented in this figure are the day 4 data without chloride for reference (taken approx. 2 hours before Cl^- addition). As shown in Figure 6a, a small change in the low frequency impedance and, correspondingly, a change in f_{L} is observed after the addition of Cl^- . This change is attributed to a decrease in the polarization resistance of the area exposed by the pre-existing defects in the DLC, R_{ct} . An example of these defects can be seen in Figure 7. Impedance data were taken every 24 hours for the next 4 days. During this time the low frequency impedance continued to decrease as shown in the day 8 data. Furthermore, a small change in f_{H} and, correspondingly R_{corr} , was observed during the additional 4 days of exposure to Cl^- not observed in the first four days of exposure.

As in the chloride solutions above, the EIS data from the borate buffer solution can be modeled with the EC presented in Figure 3a. A typical fit is shown in Figure 8 for the day four data after the addition of Cl^- . Once again, good correlation between the model and the experimental

data exists. The fit parameters for the data taken after day 4 without Cl⁻, day 4 with Cl⁻, and day 8 with Cl⁻ are presented in Table 3. As shown in this table, a large change in R_{DLC}° and a smaller change in R_{corr}° is observed after the addition of Cl⁻ to the solution. No change in R_{IL}° is observed during the 8 day exposure period. If the observed decrease in R_{DLC}° owed solely to a change in Θ , it would necessarily be reflected in R_{IL}° and C_{IL}° ; i.e. R_{IL}° must decrease as Θ increases. This must be so as the DLC lies on top the C implanted layer. Therefore a change in R_{DLC}° without a change in R_{IL}° can only be explained if a change in the intrinsic polarization resistance R_{DLC}^i occurs after the addition of Cl⁻ to the buffer solution.

Corrosion Properties of the C-implanted Layer An anodic polarization curve for carbon implanted CVD Ni (without the DLC coating) in deaerated 0.25M NaCl is presented in Figure 9. As seen in this figure, active dissolution of the specimen occurs at all potentials more positive than the OCP. Further, a positive hysteresis is observed upon reversal of the anodic potential scan indicating surface damage. While the initial, unexposed surface was charcoal gray, the exposed surface was deep black. Scanning electron microscopy revealed that this exposed surface contained an extremely fine porosity not found in the initial surface (Figure 10a 10b). Bode magnitude and phase plots for carbon implanted CVD Ni in 0.25 M Cl⁻ are presented in Figure 11a and 11b after 1 and 21 hours of immersion. This data was taken at the OCP. No dc polarization of the sample was employed. As can be seen in both the magnitude and phase data, a second time constant not resolved at early immersion times is clearly visible in the 21 hr. data. The appearance of this second time constant is consistent with the formation of pores in the implanted surface[22,23,24,25]. As was the case in the potentiodynamic experiment, upon removal of the sample from the test solution the surface morphology and color had changed from a smooth, gray surface prior to exposure, to a rough, black surface after exposure.

X-ray photoelectron measurements of the unexposed and exposed surfaces reveal two very different concentrations of Ni as a function of depth. As shown in the XPS sputter profile of Figure 12a, the initial surface C concentration is more than 80 at.% while that of Ni is less than 5 at%. Between approximately 6 and 12 minutes of sputtering the concentrations of both C and Ni level off near 50 at%. The C KLL Auger transition lineshape over this sputtering range does not

vary and, as shown in Figure 12b, indicates a strong Ni-carbide component[26]. In contrast, the sputter profile for the exposed sample is drastically different from the unexposed sample (Figure 13a). During the first 16 minutes of sputtering the concentrations of both C and Ni in the exposed sample remain close to their initial values, near 80 and 15 at%, respectively. As seen in the C KLL Auger transition data in Figure 13b, over the 6 to 12 minute sputtering interval the lineshape for this sample resembles that for graphitic or amorphous carbon [26,27].

The AES C KLL lineshapes were also consistent with the XPS data for the C 1s transition. In the early stages of sputtering, the C 1s transition in both samples had a high binding energy contribution (>284.3 eV). This suggests C-H or some C-O bonding to remnant oxygen. Over the 6 to 12 minute sputtering interval, the XPS C 1s peak for the exposed surface was observed at a binding energy of 284.3 eV. This peak was attributed to dominant graphitic/amorphous carbon bonding and agrees well with the reported literature value of 284.5 eV[19]. For the unexposed surface, the C 1s transition was observed at a binding energy of 283.3 eV in this sputtering interval. Although this peak is 0.6 eV lower than the literature value for Ni_3C (283.9 eV), it is generally in the energy range of associated with carbide bonding. Moreover, because ion implantation is a non equilibrium technique, stoichiometric Ni_3C is not expected. This may account for the difference between the binding energy observed here and the literature value for Ni_3C .

Collectively these results indicate that in Cl^- environment, the preferential dissolution of Ni from the implanted layer occurs at the OCP as well as at more anodic potentials. This process leaves behind a porous carbon rich layer with a graphitic amorphous bonding configuration. At the OCP this preferential dissolution likely owes to the galvanic interaction between Ni-rich and C-rich deposits in the implanted layer. The preferential dissolution of Ni from the implanted layer at the bottom of pre-existing defects in the DLC coatings (Figure 7) at the OCP may explain the observed gradual decrease in the R_{corr}' with time in the borate buffer solution after the addition of Cl^- as noted above. Recall that the decrease in R_{corr}' and R_{DLC}' occurred without a change in R_{IL}' or C_{IL}' that is, it occurred independent of Θ indicating R_{corr}^0 may not be an intrinsic value.

Mixed Potential Theory: interactions between DLC and Ni The galvanic current and potential relationships that may be established between the boldly exposed DLC and the base of a

pore, are presented in the mixed potential plot of Figure 14. Several scenarios are presented in this diagram. The current response as a function of applied cathodic potential for DLC coated CVD Ni in deaerated 0.25M NaCl is overlaid with: 1) the anodic behavior for CVD Ni in the bulk environment (deaerated 0.25M NaCl, pH 7), 2) the anodic behavior for CVD Ni in a simulated critical propagation solution: deaerated 1.0M NiCl₂ (2N Cl⁻, pH 6) and, 3) the anodic behavior for C implanted CVD Ni in the bulk environment. The current in the cathodic curve has been multiplied by a factor of x1000 to reflect a larger cathode area. In reality this ratio is probably closer to 10,000:1. As shown in this figure, Ni is spontaneously passive in 0.25M NaCl solution[28,29]. The couple potential formed between CVD Ni in 0.25M NaCl and DLC in this environment is high (-0.130V vs SCE) and lies in the passive region of the polarization curve for CVD Ni (Table 4). Hence, if CVD Ni were exposed at the base of a defect it should be immune to breakdown in this scenario. Because this plot does not take into account effects of the geometric solution resistance (IR) of the defect the actual couple potential may be somewhat less. Because Ni is spontaneously passive in this solution, IR will not effect the corrosion rate. It may be noted that anodic polarization of the DLC results in low current densities over a broad potential range as observed by other investigators[30]

Also presented in Figure 14 is the anodic polarization curve for CVD Ni in a subsaturated NiCl₂ solution. As seen in this figure the pitting potential for CVD Ni is greatly reduced over that in 0.25 M Cl⁻ and is equal to the OCP. Correspondingly, the couple potential formed between CVD Ni in the subsaturated NiCl₂ and DLC in 0.25M NaCl is approximately -0.239V vs SCE approximately, 0.160V more positive than the pitting potential of CVD Ni in this environment (Table 4). This potential is close to that observed for the DLC coated CVD Ni after 24 hrs. of immersion in 0.25M NaCl as noted above.

Breakdown Mechanism for DLC Coatings in Cl⁻ Environment It has been demonstrated that the DLC coatings investigated in this paper contain small defects, or pores, which are a result of the deposition process. Further, it is likely that these defects expose the C implanted Ni substrate to the bulk solution. It has also been demonstrated that in the bulk Cl⁻ environment, the C implanted Ni substrate is susceptible to preferential dissolution of Ni from the matrix at the OCP.

Furthermore, the corrosion rate of the implanted layer is increased by coupling to the DLC as shown in Figure 14 (Table 4). While this may explain the initial stages of breakdown, coating failure was not observed in the Cl⁻ solution buffered with sodium borate. Therefore, initiation of breakdown is likely aided by the development of an occluded cell chemistry, observed in pitting[31,32] and crevice corrosion[33,34], which does not develop in the buffered chloride solution.

Initially, both active dissolution of Ni and oxygen reduction take place inside a preexisting defect. However, because oxygen diffusion into the defect is restricted, deoxygenation of the defect eventually occurs. Because the DLC is capable of supporting electron transfer reactions (albeit at a low rate) once the pore solution is depleted of oxygen, the reduction reaction occurs at the DLC / solution interface, the boldly exposed material. The only reaction which remains in the defect is Ni dissolution. Because it is necessary to maintain charge neutrality inside the defect, in the absence of OH⁻ production, Cl⁻ will migrate in to the defect increasing the concentration in the defect over that of the bulk solution. Once the Cl⁻ concentration has increased sufficiently, the pitting potential of the CVD Ni will be decreased to the galvanic couple potential. This is believed to be the controlling factor in the initiation process as acidification of the occluded cell via Ni hydrolysis will not lower the pH of the defect much below pH 6[35]. This may seem contradictory to the observation that breakdown did not occur in the buffered solution. However, it may be argued that the role of the borate anions is not to maintain a neutral pH, but instead, compete with Cl⁻ migration into the defect. Hence, the critical “breakdown” concentration of Cl⁻ is not obtained in the buffer solution.

To summarize, the breakdown of DLC coatings in Cl⁻ solutions is believed to be micron sized defects in the DLC coating which are formed during the deposition process. These defects exposed the C implanted Ni layer at their base which is susceptible to preferential dissolution of Ni in the bulk solution. Because of restricted mass transport oxygen is depleted from the defect and separation of the anodic and cathodic reaction occurs. A galvanic couple is then established between the boldly exposed DLC and the C implanted Ni layer at the base of a defect. In the absence of OH⁻ production, Cl⁻ migrates into the defect to maintain charge neutrality. This rise in

Cl⁻ concentration decreases the pitting potential of the Ni below the couple potential and allows the process to become autocatalytic once only Ni is exposed at the base of the defect.

Summary

The breakdown mechanism for Plasma Source Ion Implantation diamond like carbon coatings, on CVD nickel has been investigated with electrochemical impedance spectroscopy. Examination in buffer solution revealed the presence of small defects in the DLC presumably formed in the deposition process. Breakdown of the DLC coating occurred rapidly in chloride solution, however, breakdown failed to initiate in chloride solution buffered with sodium borate.

It was concluded that the first step in the breakdown mechanism is the preferential dissolution of Ni from the C implanted layer at the bottom of a pore in the DLC. Though both the Ni dissolution and oxygen reduction reactions may initially occur simultaneously inside the pore, due to restricted diffusion, oxygen is eventually depleted from the pore. Because the exposed DLC is capable of supporting the cathodic reaction and only anodic reactions are taking place in the pore a galvanic couple is established. To maintain charge neutrality (in the absence of hydroxyl formation) Cl⁻ must migrate into the pore causing the chloride concentration to increase such that the pitting potential of Ni is decreased to that of the couple potential. This formation of a critical propagation solution is considered to be the second step in the breakdown process and must occur to maintain the corrosion reaction, else, the Ni substrate will passivate.

Because the PSII process allows the DLC composition and properties to be tailored, it may be possible to delay or lessen the severity of its breakdown in Cl⁻ environments. For example, deposition of a continuous defect free DLC layer. Although it is also possible to reduce the conductivity of the DLC, this exposed surface will always be able to support a relatively large cathodic current, i.e. the cathode to anode ratio will always be high. Therefore, it is not anticipated that altering the DLC conductivity would greatly effect the onset of breakdown.

Acknowledgments

The authors would like to thank G.G. Miller for supplying the CVD nickel and B.P. Wood and C.M. Munson for making the DLC coatings. Work on this project was funded under the auspices of the U.S. Department of Energy.

References

- 1 J. Robertson, **Progress in Solid State Chemistry**, vol. 21, no. 1, pp. 199- , 1991
- 2 K.C. Walter, M. Nastasi, H. Kung, P.Kodali, C. Munson, I. Henins, B.P. Wood, "Diamond-Like Carbon Deposition for Tribological Applications at Los Alamos National Laboratory", in *Materials Research Society Symposium Proceedings, Volume 383*, MRS, Pittsburgh, pp 411-22, 1995.
- 3 A.H. Al-Saffar, V. Ashworth, A.K.O. Bairamov, D.J. Chivers, W.A. Grant, R.P.M. Procter, vol. 20, no. 1, pp. 127-34, 1980.
- 4 Ashworth, V., R.P.M. Procter, and W.A. Grant, "The Application of Ion Implantation to Aqueous Corrosion" in *Ion Implantation*, ed. J.K. Hirvonen, Academic Press (1980), New York.
- 5 P.M. Natishan, E. McCafferty, G.K. Hubler, **The Journal of the Electrochemical Society**, vol. 135, no. 2, pp. 321-327, 1987.
- 6 C.R. Clayton, in *Passivity of Metals and Semiconductors*, eds. M. Froment, Elsevier (1983), Amsterdam, pg. 305.
- 7 Bonora, P.L. (1985) *Mater. Sci. Eng.* 69 p253
- 8 R. Valori and G.K. Hubler, (1981) *NRL Memorandum Report* 4527, 99.
- 9 Hubler, G.K., P. Trzaskoma, E. McCafferty, and I.L. Singer (1982) *Ion Implantation into Metals*, eds. V. Ashworth, W.A. Grant and R.P.M. Procter (Pergamon Press) p.24
- 10 Akavipat, S., E.B. Hale, C.E. Habermann and P.L. Hagans (1985) *Mater. Sci. Eng.* 69, p.311
- 11 P. Munn and G.K. Wolf, (1985) *Mater. Sci. Eng.* **69**, 303.
- 12 Wang, R. and J.L. Brimhall, (1984) *Ion Implantation and Ion Beam Processing of Materials*, eds. G.K. Hubler, O.W. Holland, C.R. Clayton, and C.W. White (North-Holland, New York) p.729
- 13 R.L.C. Wu, **Surface and Coatings Technology**, vol. 51, pp. 258-66, 1992.
- 14 A. Anitlla, in *Structure-Property Relationships in Surface Modified Ceramics*, Kluwer Academic, pp. 455-75, 1989.
- 15 T.J. Bowles, P.J. Doe, A. Hime, R.G.H. Robertson, T.C. Spencer, P.M. Thornewell, J.B. Wilhelmy, J.F. Wilkerson, LANL Report no. FIN-94--ER-E324, Los Alamos National Laboratory, 1992.
- 16 D.P. Butt, K.C. Walter, M. Nastasi, A.L. Campuzano, P.S. Martin, B.P. Wood, D.J. Rej, G.G. Miller, **Philosophical Magazine Letters**, vol. 70, no. 6, pp. 385-87, 1994.
- 17 M. Nastasi, J.P. Hivonen, G.M. Pharr, W.C. Oliver, **Journal of Materials Research**, vol. 3, no. 2, pp. 226-32, 1988.
- 18 K.C. Walter, M. Nastasi, H. Kung, P. Kodali, C. Munson, I. Henins, B.P. Wood, "Diamond-Like Carbon Deposition for Tribological Applications at Los Alamos National Laboratory", *Materials Research Society Symposium Proceedings*, vol. 383, 1995.

- 19 J. F. Moulder, W. F. Stickle, P. E. Sobol, and K. E. Bomben, *Handbook of X-ray Photoelectron Spectroscopy*, Physical Electronics Division, Perkin-Elmer Corp., Eden Prairie, MN, 1992
- 20 J. Hitzig, K. Juttner, W.J. Lorenz, W. Paatsch, **The Journal of the Electrochemical Society**, vol. 133, no. 5, pp. 887-92, 1986.
- 21 F. Mansfeld, M.W. Kendig, **The Journal of the Electrochemical Society**, vol. 135, no. 4, 1988.
- 22 M. Kendig, J.R. Scully, **Corrosion**, vol. 46, no. 1, pp. 22-29, 1990.
- 23 H.P Hack, J.R. Scully, **The Journal of the Electrochemical Society**, vol. 138, no. 1, pp. 33-40, 1991
- 24 R. Hirayama, S. Haruyama, **Corrosion**, vol. 47, no. 12, pp. 952-958, 1991.
- 25 F. Mansfeld, C.H. Tsai, **Corrosion**, vol. 47, no. 12, pp. 958-63, 1991.
- 26 J. P Coad and J. C. Rivière, **Surface Science**, vol. 25, pp. 33-40, 1971
- 27 A. K. Green and V. Rehn, **J. Vac. Sci. Technol.**, vol. A1, no. 4, pp.1877-1879, 1983
- 28 B. MacDougall, M.J. Graham, **Journal of the Electrochemical Society**, vol. 131, no. 4, pp. 727-30, 1984.
- 29 K.S. Lei, D.D. Macdonald, B.G. Pound, B.E. Wilde, **Journal of the Electrochemical Society**, vol. 135, no. 7, pp. 1625-32, 1988.
- 30 P.M. Natishan, E. McCafferty, E.P. Donovan, G.K. Hubler, *Advances in Coating Technologies for Corrosion and Wear Resistant Coatings*, A.R. Srivatsa, C.R. Clayton, J.K. Hirvonen eds., The Minerals, Metals & Materials Society, pp. 223-31, 1995.
- 31 K.J. Vetter, H.H. Strehblow, "Pitting Corrosion in an Early Stage and its Theoretical Implications", in Localized Corrosion, R.W. Staehle, B.F. Brown, J. Kruger, A. Argawal eds., NACE, Houston, pp. 240-51, 1974.
- 32 J.R. Galvele, **The Journal of the Electrochemical Society**, vol. 123, no. 4, pp. 464-74, 1976.
- 33 J.W. Oldfield, W.H. Sutton, **British Corrosion Journal**, vol. 13, no. 1, pp 13-22, 1978.
- 34 B.A. Shaw, "The Importance of Ohmic Drop In Crevice Corrosion", in ASTM STP 1056, L.L. Scribner, S.R. Taylor eds., ASTM, Philadelphia, pp. 211-19, 1990.
- 35 M. Pourbaix, Atlas of Electrochemical Equilibria in Aqueous Solutions, NACE, Houston, 1974.

List of Tables

Table 1 Selected Corrosion Resistant Alloys Produced by Ion Implantation

Table 2 Select parameters from CNLS fitting of EIS data for DLC Ni in 0.25M NaCl as a function of immersion time. Also presented is the % area of the surface covered by defects (Θ) as a function of time calculated from Eq.1 (total area=1.2 cm²).

Table 3 Parameters from CNLS fitting of EIS data for DLC Ni in sodium Borate buffered solution and sodium Borate buffered solution after the addition of 0.25M NaCl as a function of immersion time. Data taken after 1 hr and 96 hrs in borate solution were identical.

Table 4 Open circuit potential, pitting potential and, possible galvanic current and potential relationships that may be established between the boldly exposed DLC and the base of a pore (from Figure 14). In Figure 14, the cathodic current from the DLC in 0.25M NaCl was multiplied by a factor of x1000 to reflect a larger cathodic area.

Table 1 Selected Corrosion Resistant Alloys Produced by Ion Implantation

Material Studied	Ions; Energy (keV); Dose (ions/cm²)	Results, Comments	Reference
Fe	B, N; 30 - 50 keV; 1×10^{16}	Lower corrosion rates in acid and acidic chloridemedias	Bonora (1985)
Fe	Cr; 20 keV; $0.5-2 \times 10^{17}$	Ion implantation (Cr) alloyed surface behaves electrochemically like conventional alloy (stainless steel).	[Ashworth, et al (1980)]
52100, M50	Cr,Cr+P,Mo,Ta; 150 keV; 2×10^{17}	Pitting corrosion of bearing alloys substantially improved.	[Valori and Hubler,(1981); Wang et al., 1979]
52100	Ti; 190 keV; 4.6×10^{17}	Ti implantation produces an amorphous alloy with improved corrosion resistance	Hubler et al. (1982)
AZ91C (an Mg alloy)	Fe; 100 keV; $1 - 2 \times 10^{17}$	improvement in pitting resistance by lowering the galvanic action of second-phase particles	Akavipat et al (1985)
304 SS, 316SS	P; 40 keV; 10^{17}	P implantation produces amorphous surface alloy with high corrosion resistance.	[Clayton et al, (1983), Whitton et al., 1978;]
Ti	Pd; 75 keV; 10^{16}	Noble metal implants effective for passivation; corrosion I reduced >1000 X in strong acid; results confirm corrosion mechanism in bulk Ti/noble metal alloys.	[McCafferty and Hubler, (1978)]
Ti	Pd; 200 keV; $10^{16}/\text{cm}^2$	Crevice corrosion resistance improved.	[.Munn and Wolf, (1985)]
Al 7075-T6	Mo; 20keV; $10^{17}/\text{cm}^2$	Mo implantation significantly improves the pitting resistance in pure Al and a similar, though less marked effect is observed in the alloy	Al-Saffar et al. (1980)
Al	Mg, Cr, Si, Zr, Nb, Mo, Zn; 20 - 90 keV; $0.3 - 8.0 \times 10^{16}/\text{cm}^2$	Si, Cr, Zr, Nb, and Mo produced surface oxides with higher pitting potentials than pure Al, while Zn produced a surface oxide with a pitting potential lower than Al, and Mg produce a surface oxide with the same potential as Al.	Natishan et al. (1988)
NiTi	Ni; 2.5 - 5.0 MeV; 2×10^{15}	Ni implantation produces amorphous surface alloy showing significant improvements in localized corrosion resistance	Wang and Brimhall

Table 2 Select parameters from CNLS fitting of EIS data for DLC Ni in 0.25M NaCl as a function of immersion time. Also presented is the % area of the surface covered by defects (Θ) as a function of time calculated from Eq.1 (total area=1.2 cm²).

Immersion Time (hrs)	R_{corr}° (ohms)	C_{dl}° (Farads)	R_{IL}° (ohms)	R_{DLC}° (ohms)	$\Theta \times 100$ % defect	$(1-\Theta) \times 100$ % DLC
1	1.14 x10 ⁴	1.58 x10 ⁻⁸	1.13 x10 ⁴	5.89 x10 ⁶	0.003	99.997
24	2.51 x10 ³	6.63 x10 ⁻⁸	1.13 x10 ⁴	1.44 x10 ⁶	0.02	99.98
28	489	1.26 x10 ⁻⁷	1.07 x10 ⁴	2.91 x10 ⁶	0.08	99.92

Table 3 Parameters from CNLS fitting of EIS data for DLC Ni in sodium borate buffered solution and sodium borate buffered solution after the addition of 0.25M NaCl (at 96.5 hrs) as a function of immersion time. Data taken after 1 hr and 96 hrs in borate solution were identical.

Immersion Time (hrs)	R_{corr}° (ohms)	C_{dl}° (Farads)	R_{IL}° (ohms)	C_{IL}° (ohms)	R_{DLC}° (ohms)	C_{DLC}° (ohms)
1 and 96 (borate)	4.57×10^3	2.30×10^{-6}	1.60×10^5	2.45×10^{-9}	2.65×10^5	5.28×10^{-6}
96.5 (borate+Cl)	4.08×10^3	2.89×10^{-6}	1.60×10^5	2.45×10^{-9}	8.54×10^4	2.93×10^{-5}
192 (borate+Cl)	4.07×10^3	3.25×10^{-6}	1.60×10^5	2.45×10^{-9}	7.90×10^4	5.28×10^{-5}

Table 4 Open circuit potential, pitting potential and, possible galvanic current and potential relationships that may be established between the boldly exposed DLC and the base of a pore (from Figure 14). In Figure 14, the cathodic current from the DLC in 0.25M NaCl was multiplied by a factor of x1000 to reflect a larger cathodic area. The OCP for DLC CVD Ni is also presented for reference.

Material / Environment	Open circuit potential (V vs SCE)	Pitting potential (V vs SCE)	Couple potential w/ DLC (V vs SCE)	Couple current w/ DLC (Amps)
DLC / 0.25M NaCl	-0.104	- NA -	- NA -	- NA -
DLC-CVD Ni / 0.25M NaCl	-0.217	- NA -	- NA -	- NA -
CVD Ni / 0.25M NaCl	-0.390	+0.295	-0.130	1.5x10 ⁻⁶
CVD Ni / 1.0M NiCl₂	-0.400	-0.400	-0.239	7.0x10 ⁻⁵
C-implant CVD Ni / 0.25M NaCl	-0.175	-0.175	-0.112	8.0x10 ⁻⁷

List of Figures

Figure 1 Bode **a)** magnitude and **b)** Bode phase plots for DLC coated CVD Ni in deaerated 0.25M NaCl solution after 1 hr, 24 hrs, and 28 hrs of immersion.

Figure 2 **a)** SEM micrograph of corrosion pit formed in Cl⁻ solution (planar view) and **b)** optical micrograph of similar corrosion pit in cross-section.

Figure 3 **a)** Schematic diagram representing the layers in DLC coating and a defect native to the coating **b)** electrical equivalent circuit model representing the breakdown of DLC coated CVD Ni in NaCl solution.

Figure 4 CNLS fits of EC in Figure 5b for DLC coated CVD Ni in 0.25M NaCl after 24 hrs of immersion (Figure 3). Showing Bode magnitude and phase data.

Figure 5 **a)** Bode magnitude and **b)** Bode phase plots for DLC coated CVD Ni in deaerated borate buffer solution after 1 hr and 4 days of immersion.

Figure 6 Bode **a)** magnitude and **b)** phase plots for DLC coated CVD Ni in deaerated borate buffer solution without Cl⁻ after 4 days and with Cl⁻ after 1 hr and 4 days of immersion.

Figure 7 A native defect in DLC coated CVD Ni found in the coating after deposition but prior to immersion in test solution.

Figure 8 Bode magnitude and phase plots from CNLS fits of EC in Figure 5 for DLC coated CVD Ni in sodium borate buffered solution (day 4) after the addition of 0.25M Cl⁻.

Figure 9 Anodic polarization curve for carbon implanted CVD Ni in deaerated 0.25M NaCl.

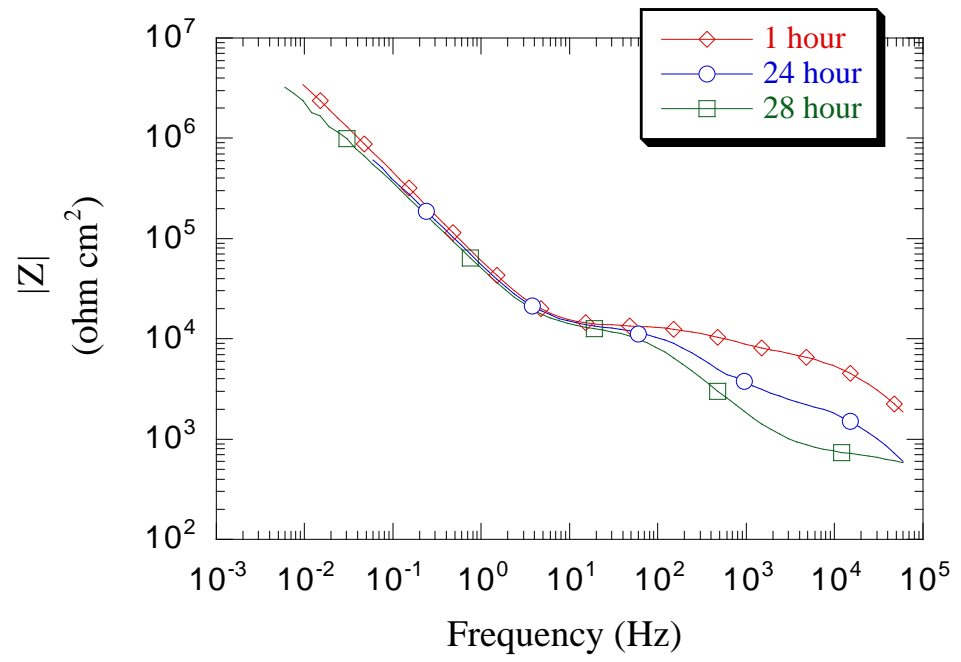
Figure 10 SEM micrographs of the carbon implanted surface **a)** prior to immersion and **b)** after immersion in 0.25M Cl⁻ and polarization to 0.200V SCE.

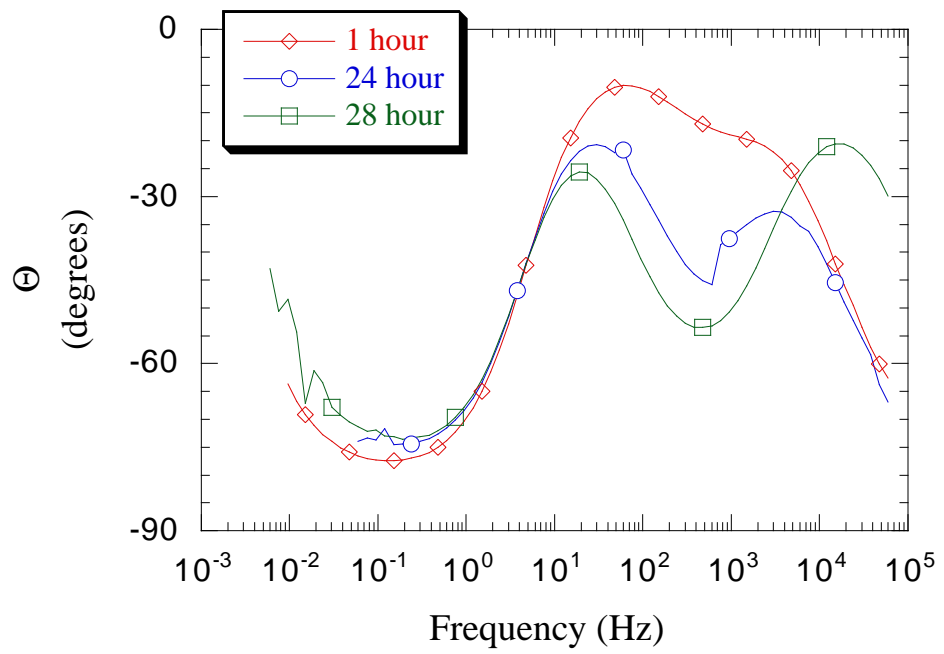
Figure 11 **a)** Bode magnitude and **b)** Bode phase plots for carbon implanted CVD Ni in deaerated borate buffer solution after as a function of immersion. Note appearance of second time constant after 21 hrs of immersion.

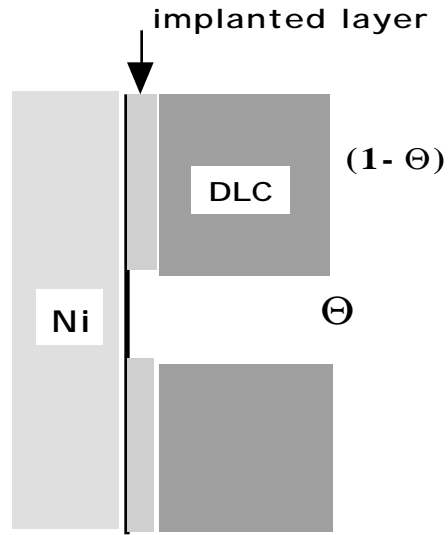
Figure 12 **a)** XPS sputter profile of carbon implanted CVD Ni prior to immersion in test solution. **b)** Auger line shape for C KLL on the same pre-immersion surface after 12 minutes of sputtering.

Figure 13 **a)** XPS sputter profile of carbon implanted CVD Ni after immersion and polarization in test solution. **b)** Auger line shape for C KLL on the same post-immersion surface after 12 minutes of sputtering.

Figure 14 Mixed potential diagram showing the possible galvanic interactions between DLC in 0.25M Cl⁻ (ambient aeration) and 1) CVD Ni in deaerated 0.25M Cl⁻, 2) CVD Ni in deaerated 1M NiCl₂ (2N Cl⁻) and, 3) the anodic behavior for C implanted CVD Ni in the bulk environment. The cathodic curve (DLC) has been multiplied by a factor of x1000 to reflect a larger cathode area.







Θ pore surface coverage
 $(1-\Theta)$ DLC surface coverage

